

Floquet insulators and lattice fermions

Thomas Iadecola,^{1, 2, *} Srimoyee Sen,^{1, †} and Lars Sivertsen^{1, ‡}

¹*Department of Physics and Astronomy, Iowa State University, Ames, Iowa 50011, USA*

²*Ames National Laboratory, Ames, Iowa 50011, USA*

(Dated: June 30, 2023)

Floquet insulators are periodically driven quantum systems that can host novel topological phases as a function of the drive parameters. These new phases exhibit features reminiscent of fermion doubling in discrete-time lattice fermion theories. We make this suggestion concrete by mapping the spectrum of a noninteracting (1+1)D Floquet insulator for certain drive parameters onto that of a discrete-time lattice fermion theory with a time-independent Hamiltonian. The resulting Hamiltonian is distinct from the Floquet Hamiltonian that generates stroboscopic dynamics. It can take the form of a discrete-time Su-Schrieffer-Heeger model with half the number of spatial sites of the original model, or of a (1+1)D Wilson-Dirac theory with one quarter of the spatial sites.

Zero-energy fermionic modes, or zero modes, are among the earliest manifestations of topology in quantum many-body theory. In systems with a gapped bulk, they appear localized at topological defects like solitons and vortices, or as dispersive modes at boundaries between phases with different bulk topological invariants [1]. They can carry fractional charges under global symmetries and manifest fractional or non-Abelian statistics when braided [2–7], and their existence enforces degeneracies in the many-body spectrum [8, 9].

Quantum systems driven periodically in time, known as Floquet systems, furnish intrinsically nonequilibrium generalizations of topological and conventionally ordered phases [10–21]. Despite lacking energy conservation, they retain a notion of eigenstates and eigenvalues when observed at “stroboscopic times” that are integer multiples of the driving period T . Instead of an energy spectrum which can in principle be unbounded in the thermodynamic limit, stroboscopic dynamics and eigenstates are characterized by a bounded spectrum of quasienergies $-\pi/T \leq \epsilon < \pi/T$ that are only conserved modulo $\frac{2\pi}{T}$. The periodic nature of quasienergy furnishes a generalization of zero modes. For example, fermionic Floquet systems known as Floquet insulators can exhibit localized “ π modes” whose existence implies a “ π pairing” between many body states at quasienergy ϵ and $\epsilon + \frac{\pi}{T}$ [22–27].

Another setting in which π modes arise is spacetime lattice regularizations of fermionic quantum field theories. In particular, discretizing the Dirac operator on a spacetime lattice leads to the so-called fermion doubling problem, where the total number of fermionic degrees of freedom increases by a factor of 2^D , where D is the spacetime dimension [28, 29]. The extra modes, known as “doublers,” are undesirable and several methods, including Wilson, Kogut-Susskind, and domain-wall fermions [30–35], are commonly used to dispense with them. Nevertheless, it is natural to ask whether the doubler modes

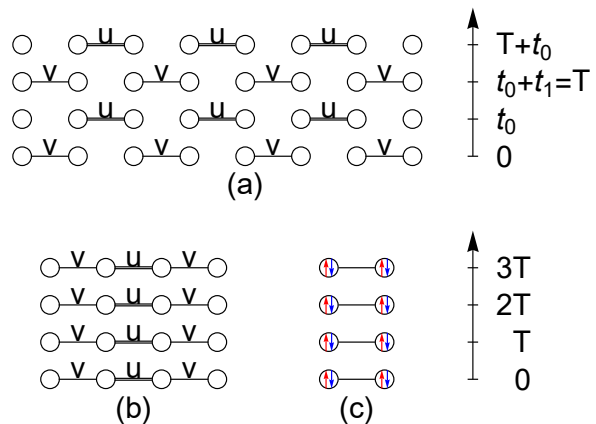


FIG. 1. Schematic of the mapping between stroboscopic Floquet dynamics and time-independent lattice Hamiltonians. The spectrum of the stroboscopic dynamics corresponding to Eq. (6), shown in (a), can be mapped onto that of a discrete-time Su-Schrieffer-Heeger (b) or Wilson-Dirac (c) theory. The number of spatial sites in (b) is halved with respect to (a) to accommodate the additional degrees of freedom due to fermion doubling. The number of sites are further halved in (c) to accommodate the spinful nature of the Wilson-Dirac fermions (depicted via arrows inside the lattice sites).

associated with zero modes, which occur at frequency $\frac{\pi}{\tau}$ where τ is the temporal lattice spacing, are related to the π modes that can appear in Floquet insulators.

In this paper, we answer this question affirmatively for a particular (1+1)D Floquet-insulator model. Specifically, we show that the quasienergy spectrum of a continuous-time Floquet model of spinless complex fermions can be mapped directly onto the spectrum of discrete-time lattice fermions with a time-independent Hamiltonian. The lattice spacing of this discrete time theory equals the driving time period T of the Floquet system. The mapping is made easier by the observation that the Dirac equation takes the form of a Schrödinger equation for the corresponding fermion Hamiltonian. The lattice fermion model can take the form of a Su-Schrieffer-Heeger (SSH) model with half

* iadecola@iastate.edu

† srimoyee08@gmail.com

‡ lars@iastate.edu

the spatial lattice sites of the Floquet model, or of a Wilson-Dirac model with one quarter of the sites. Furthermore, for appropriately chosen solutions of the mapping between spectra, the phase diagrams of the Floquet and lattice models match. In particular, the topological phase of the Floquet model, which exhibits localized zero and π modes with open boundary conditions, coincides with the topological phase of the related lattice Hamiltonians, where π modes appear as doublers of zero modes. While previous studies [36, 37] have used Floquet systems to provide new perspectives on lattice fermion doubling, here we focus on exposing a direct correspondence between the two.

Lattice fermion doubling.—A continuous-time free-fermion theory in Minkowski space with Hamiltonian H has the fermion/Dirac operator $\gamma_0(i\partial_t - H)$ from which we can extract the Schrödinger operator $i\partial_t - H$. The eigenvalues of this operator are $\pm\sqrt{p_0^2 - E^2}$, where p_0 is the Fourier variable conjugate to time t and E are the eigenvalues of H [38]. The zeroes of these eigenvalues at $p_0 = E$ correspond to poles of the fermion propagator $(i\partial_t - H)^{-1}\gamma_0^{-1}$. Discretizing time in this theory leads to fermion doubling [28, 29]. To see this, let τ be the lattice spacing in the time direction. The poles of the discrete-time theory now satisfy $\frac{1}{\tau}\sin(p_0\tau) = E$, which leads to two solutions:

$$p_0 = \frac{1}{\tau}\sin^{-1}(E\tau) \quad \text{and} \quad p_0 = \frac{\pi}{\tau} - \frac{1}{\tau}\sin^{-1}(E\tau) \quad (1)$$

Thus, for every pole of the continuous-time propagator there are two poles of the discrete-time propagator [39–42]. In particular, for a zero mode of the continuous-time theory, the discrete-time theory has modes at $p_0 = 0$ and $p_0 = \frac{\pi}{\tau}$; the new π mode arises purely due to time discretization.

A corresponding phenomenon is also observed in Euclidean-time lattice field theory [43] [44]. There, the Schrödinger operator in continuous time has eigenvalues $\pm\sqrt{p_0^2 + E^2}$, which, unlike the Minkowski theory, vanishes only at $p_0 = E = 0$. In this case, upon discretizing time, fermion doubling manifests itself as a degeneracy of Schrödinger eigenvalues. For instance, any eigenstate $|p_0, E\rangle$ with eigenvalue $\frac{1}{\tau}\sqrt{\sin^2(p_0\tau) + E^2}$ has a partner $|\frac{\pi}{\tau} - p_0, E\rangle$ with the same eigenvalue. In congruence with the Minkowski-space analysis, if the continuous-time fermion propagator has a pole at $p_0 = E = 0$, then there is another pole at $p_0 = \pi/\tau$. More interestingly, the states $|E, E\rangle$, which correspond to the energy eigenstates of H , have the same spatial profiles in the position eigenbasis as $|\frac{\pi}{\tau} - E, E\rangle$. Therefore, if H has a spatially localized zero mode, the corresponding discrete-time Schrödinger equation has two solutions with the same spatial profile.

In this paper, we will consider real-time (i.e., Minkowski) theories as opposed to imaginary-time (Euclidean) ones, as the comparison between the Floquet and lattice spectra is more natural for the former. However, there is no fundamental obstruction to performing a sim-

ilar analysis for Euclidean theories, and such an approach may be desirable when generalizing beyond the case of noninteracting fermions, which is our focus here. We will briefly mention how the comparison between Floquet systems and lattice fermions in Minkowski spacetime can be adapted for Euclidean spacetime lattices.

Floquet insulator model.—As a simple example of a Floquet insulator, we consider a continuous-time (1+1)D model on a spatial lattice of $2N$ sites defined by the evolution operator

$$U(t) = \begin{cases} e^{-iH_0 t} & \text{for } 0 < t < t_0 \\ e^{-iH_1(t-t_0)}e^{-iH_0 t_0} & \text{for } t_0 \leq t < t_0 + t_1 \end{cases}, \quad (2)$$

with

$$\begin{aligned} H_0 &= 2 \sum_{j=0}^{N-1} (a_{2j}^\dagger a_{2j+1} + \text{H.c.}) \\ H_1 &= 2 \sum_{j=0}^{N-1} (a_{2j+1}^\dagger a_{2j+2} + \text{H.c.}), \end{aligned} \quad (3)$$

where a_i is a fermion annihilation operator on site $i = 0, \dots, 2N - 1$. Unless otherwise specified, we consider periodic boundary conditions (PBC) such that $a_{2N} \equiv a_0$. The Hamiltonians in Eq. (3) are the “trivial” and “topological” parts of the (static) SSH model [2, 45],

$$H_{\text{SSH}} = \frac{u}{2}H_1 + \frac{v}{2}H_0. \quad (4)$$

The energy spectrum of this model with PBC is given by

$$E_{\text{SSH}}(k) = \pm\sqrt{u^2 + v^2 + 2uv\cos(2k)}, \quad (5)$$

where $0 \leq k < \pi$ is the crystal momentum and we have set the spatial lattice spacing to 1. The SSH model has a symmetry-protected topological (SPT) and a trivial phase that have identical bulk spectra. The two gapped phases can be distinguished by their energy spectra in open boundary conditions (OBC): in the SPT phase there are two spatially localized zero modes pinned to the middle of the energy gap, one at each end of the chain, while in the trivial phase there are none. Expanding the model around $k = \frac{\pi}{2}$ yields a Dirac fermion theory with a mass proportional to $u - v$; the transition between the SPT and trivial phases occurs at the massless point $u = v$. H_0 and H_1 can be viewed as representatives of the trivial and SPT phases, respectively.

The Floquet model (2) is closely related to a simple (1+1)D model discussed in Refs. [24, 27, 46], with the small difference that Eq. (2) is formulated in terms of complex rather than Majorana fermion operators [47]. The analysis of both models is nearly identical, and they have the same phase diagram. Since energy is no longer conserved in the time-dependent model (2), phases are classified according to spectral properties of the Floquet operator

$$U_{\text{F}} = U(T) = e^{-iH_1 t_1} e^{-iH_0 t_0} \equiv e^{-iH_{\text{F}} T}, \quad (6)$$

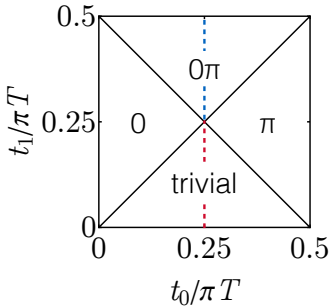


FIG. 2. Phase diagram of the Floquet model (6). The phases are labeled by the presence or absence of zero and π modes localized to boundaries. This work focuses on the vertical dashed line at $\frac{t_0}{T} = \frac{\pi}{4}$, which passes through the trivial and 0π phases.

where $T = t_0 + t_1$ is the driving period and $H_F = \frac{i}{T} \ln U_F$ is known as the Floquet or stroboscopic Hamiltonian. The quasienergies $-\pi/T \leq \epsilon < \pi/T$ are the eigenvalues of H_F . They can be obtained analytically because the model (6) is quadratic [47]. There are four phases, which we label trivial, 0, π , and 0π (see Fig. 2). The 0 and π phases have localized boundary modes with $\epsilon = 0$ and $\frac{\pi}{T}$, respectively; the 0π phase has both zero and π modes, while the trivial phase has neither. The phase boundaries in Fig. 2 are the lines in the t_0 - t_1 plane where the quasienergy gap closes. The trivial and 0 phases are adiabatically connected to the trivial and topological phases of the SSH model, respectively. The phases with π modes are “intrinsically Floquet” phases in the sense that they cannot arise in the absence of the drive.

Floquet to lattice mapping.—It is natural to speculate that the π modes in the Floquet system can be viewed as doubler modes of an appropriate discrete-time lattice fermion theory with time lattice constant $\tau = T$. To confirm this, we will identify a discrete-time theory with Hamiltonian H and spectrum E such that the poles in Eq. (1) are in one-to-one correspondence with quasienergy eigenvalues ϵ . Note that, in order for this identification to be possible, it is necessary that the (single-particle) spectrum of H_F exhibit a π -pairing such that for every quasienergy ϵ there is a partner at $\frac{\pi}{T} - \epsilon$. For the model (6), this feature arises along the line $\frac{t_0}{T} = \frac{\pi}{4}$, which connects the trivial and 0π phases. On this line, the quasienergy spectrum of H_F with PBC takes the form [47]:

$$\epsilon(k) = \pm \cos^{-1}[-\cos(2\eta) \cos(2k)], \quad (7)$$

where $\eta = \frac{t_1}{T} - \frac{\pi}{4}$ measures the distance from the gap closure at $\frac{t_1}{T} = \frac{\pi}{4}$. To enable a one-to-one mapping onto the poles (1), we will partition the quasienergy spectrum ϵ into two subsets containing quasienergies $\tilde{\epsilon}$ and $\frac{\pi}{T} - \tilde{\epsilon}$. We will then seek a model H whose energy spectrum E satisfies

$$E = \frac{1}{T} \sin(T\tilde{\epsilon}), \quad (8)$$

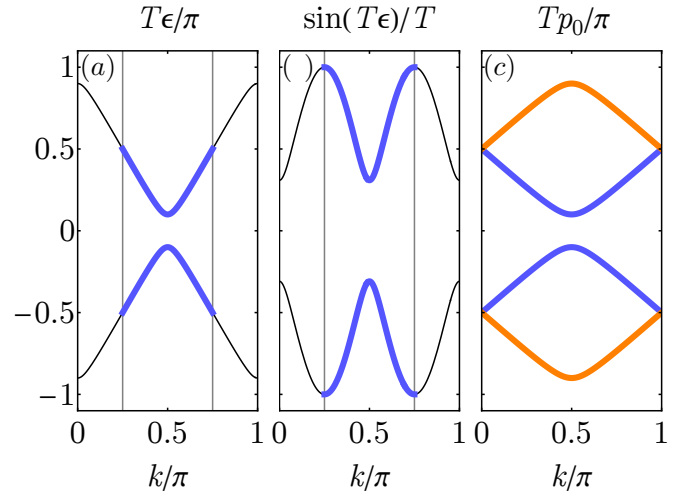


FIG. 3. Spectrum of the Floquet model and its mapping onto the lattice spectrum. (a) Quasienergy spectrum of Eq. (6) along the line $\frac{t_0}{T} = \frac{\pi}{4}$ [see Eq. (7)]. The quasienergy values highlighted in blue are those corresponding to crystal momenta k in the interval $[\frac{\pi}{4}, \frac{3\pi}{4}]$ (grey vertical lines), denoted $\tilde{\epsilon}$ in the text. (b) Sine-transformed quasienergy spectrum entering Eq. (8). (c) Pole positions p_0 with momenta assigned according to the SSH mapping. The orange bands denote doublers, which correspond to the quasienergies $\frac{\pi}{T} - \tilde{\epsilon}$.

which stems from identifying $p_0 = \tilde{\epsilon}$ in Eq. (1). A suitable choice of $\tilde{\epsilon}$ consists of the values $\epsilon(k)$ for $\frac{\pi}{4} \leq k < \frac{3\pi}{4}$ (see Fig. 3). The corresponding construction in Euclidean spacetime aims to identify the eigenvalues of the states $|E, E\rangle$ and $|\frac{\pi}{T} - E, E\rangle$ with $\frac{1}{T}\sqrt{2}\sin(T\tilde{\epsilon})$.

SSH mapping.—We now seek a Hamiltonian whose spectrum satisfies Eq. (8). Since U_F is built using the SSH-type Hamiltonians (3), we first consider an SSH Hamiltonian with dispersion given by Eq. (5). In this case, Eq. (8) can be solved by

$$E_{\text{SSH}}(k') = \frac{1}{T} \sin \left[T\epsilon \left(\frac{k'}{2} + \frac{\pi}{4} \right) \right], \quad (9)$$

where $0 \leq k' < \pi$, where

$$u = \frac{1 \pm \sin(2\eta)}{2T} \quad \text{and} \quad v = \frac{1}{T} - u. \quad (10)$$

(Note that we have assumed $u, v \geq 0$ for simplicity.)

The two possible assignments of u satisfying Eq. (9) have no impact on the bulk energy spectrum, but can nevertheless be physically distinguished by solving the SSH model with OBC. The SSH model (4) is in the SPT phase when $u > v$ and the trivial phase when $u < v$. Since the topological 0π phase of H_F occurs when $\eta > 0$, we must pick the branch of Eq. (10) such that $u > v$ when $\eta > 0$; this is accomplished by picking the “+” branch. Let \tilde{H}_{SSH} denote the resulting time-independent SSH Hamiltonian.

By construction, the doubled spectrum (1) of \tilde{H}_{SSH} when defined on a discrete-time lattice with spacing $\tau =$

T [Fig. 3(c)] matches the quasienergy spectrum of the Floquet Hamiltonian H_F [Fig. 3(a)]. Thus, \tilde{H}_{SSH} cannot be defined on the same spatial lattice as H_F ; rather, if the original Floquet model is defined on a lattice of $2N$ sites, \tilde{H}_{SSH} must be defined on N sites. To see this, recall that Eq. (9) maps the interval $\frac{\pi}{4} \leq k < \frac{3\pi}{4}$ to the interval $0 \leq k' < \pi$. The k interval contains half of the N allowed crystal momentum values for H_F , so k' can only take $\frac{N}{2}$ values (note that this requires N to be even). This corresponds to N sites because the SSH model has a two-site unit cell. Thus, \tilde{H}_{SSH} should not be interpreted as a mere rewriting of H_F . Instead, the models are related by the nontrivial procedure of fermion doubling.

Wilson-Dirac mapping.—To make more direct contact with lattice field theory, we now show that Eq. (8) can also be satisfied by the spectrum of a Wilson-Dirac (WD) Hamiltonian. The corresponding solution is inspired by the observation that the spectrum of a WD Hamiltonian with PBC can be mapped onto that of an SSH Hamiltonian with PBC. The WD Hamiltonian on a 1D spatial lattice with N sites can be written (here working in OBC for simplicity)

$$H_{\text{WD}} = \sum_{x,x'=0}^{N-1} \bar{\psi}_x \left[R \gamma_1 (-i \nabla_{x,x'}) - \frac{R}{2} \nabla_{x,x'}^2 + m \delta_{x,x'} \right] \psi_{x'}, \quad (11)$$

where $\nabla_{x,x'} = (\delta_{x',x+1} - \delta_{x',x-1})/2$ is a symmetric spatial derivative, $\nabla_{x,x'}^2 = \delta_{x'-1,x+1} + \delta_{x'+1,x-1} - 2$ is the second derivative, ψ_x is a two-component Dirac spinor with associated gamma matrices γ_0, γ_1 , and $\bar{\psi}_x = \psi_x^\dagger \gamma_0$. The energy spectrum of this model with PBC is given by

$$E_{\text{WD}}(p) = \pm \sqrt{R^2 \sin^2 p + [m + R(1 - \cos p)]^2}, \quad (12)$$

where $-\pi \leq p < \pi$. Solving Eq. (8) yields

$$E_{\text{WD}}(p') = \frac{1}{T} \sin \left[T \epsilon \left(\frac{p'}{4} + \frac{\pi}{2} \right) \right], \quad (13)$$

where $-\pi \leq p' < \pi$, provided that

$$m = \pm \frac{\sin(2\eta)}{T} \quad \text{and} \quad R = \frac{1}{2T} - \frac{m}{2}, \quad (14)$$

where we have assumed $R \geq 0$ for simplicity. Following the SSH case, we now ask which of these branches corresponds to a topological phase when $\eta > 0$. With OBC, the WD Hamiltonian (11) exhibits localized edge modes when $m < 0$ [47]. Demanding that this condition coincide with positive η selects the “-” branch. We denote the resulting time-independent Wilson-Dirac Hamiltonian by \tilde{H}_{WD} .

We have thus found a second time-independent Hamiltonian, \tilde{H}_{WD} , whose doubled spectrum when defined on a discrete-time lattice coincides with the quasienergy spectrum of H_F . We note here that \tilde{H}_{WD} must be defined

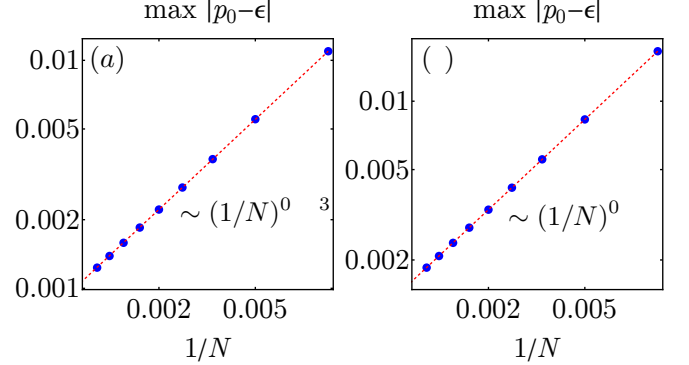


FIG. 4. Finite-size scaling of the maximum difference between discrete-time spectra p_0 and quasienergy spectra ϵ (a) for OBC and (b) for OBC with a domain wall where η switches sign. In both panels we compare to the SSH spectrum and fix $\eta = \pi/8$, considering system sizes $N = 100, 200, \dots, 900$. Dashed lines indicate best fits to power laws in $1/N$ that are consistent with the expected scaling.

on a lattice with $N/2$ sites (i.e., one quarter of the sites in the original Floquet model). Like the SSH case, the crystal momentum interval $0 \leq k < \frac{\pi}{2}$ corresponding to $\tilde{\epsilon}$ contains $\frac{N}{2}$ points; thus, so does the new crystal momentum interval $-\pi \leq p' < \pi$. However, unlike the SSH model, the WD model has a one-site unit cell, so there is one site per crystal momentum value.

Discussion.—The equalities (9) and (13) relate the discrete-time spectra of static SSH and WD models to the quasienergy spectrum of Eq. (6) with PBC. In each case, the “correct” branch of the respective model parameter solutions is chosen by matching the presence of zero modes as a function of η . However, these zero modes are properties of the OBC spectrum. Given that the PBC spectra match by construction, we expect that the OBC spectra match up to $\sim 1/N$ corrections. In Fig. 4(a) we demonstrate this numerically for the SSH mapping by plotting the system size dependence of the maximum difference between the discrete-time frequency spectrum p_0 and the quasienergy spectrum ϵ , where each spectrum is constructed as an ordered list.

Another test of equivalence is to compare spectra in the presence of a domain wall in η . For the SSH model, this corresponds to a standard domain wall in the mass profile [2], while for the WD model it amounts to a domain wall in both the mass and the Wilson parameter R . For the Floquet model, a domain wall in η entails an abrupt change in the coefficient of H_1 from 2 to $2(\frac{\pi}{4} - \eta)/(\frac{\pi}{4} + \eta)$ at some point in space. In Fig. 4(b) we examine the finite-size dependence of the difference between the discrete-time SSH and quasienergy spectra in the presence of a domain wall in the middle of the chain, again finding the expected $\sim 1/N$ scaling. These results build confidence that the mapping we develop defines a notion of equivalence in the thermodynamic limit between models irrespective of boundary conditions or the presence of topological defects.

Outlook.—We have demonstrated spectral equivalence between a simple Floquet insulator model in (1+1) dimensions and two canonical fermion models (SSH and WD) defined on a two-dimensional spacetime lattice. The mapping between spectra relies on a notion of π pairing in the single-particle spectrum, which occurs along the line $\frac{t_0}{T} = \frac{\pi}{4}$. This pairing allows us to discard half of the degrees of freedom in the Floquet model to define a related static model, which recovers the discarded eigenvalues via fermion doubling after time discretization. One interesting question for future work is whether the equivalence can be extended off the line $\frac{t_0}{T} = \frac{\pi}{4}$ [48]. We note that π pairing also occurs along the line $\frac{t_1}{T} = \frac{\pi}{4}$ for PBC but is lost for OBC, as evidenced by the separate existence of 0 and π modes with OBC. A separate direction is to consider extensions of these mappings to (2+1)D systems, where new phases like anomalous Floquet topological insulators emerge [23, 49]. In any di-

mension, it is also worth considering whether a similar equivalence between bulk topological invariants in Floquet systems [23, 50–53] and lattice field theories can emerge [54]. Finally, it will be interesting to consider whether an equivalence to lattice field theory can be formulated for interacting Floquet systems, which experience unbounded heating that requires the introduction of prethermalization or localization physics to enable long-lived phenomena [24, 55–57].

ACKNOWLEDGMENTS

TI acknowledges support from the National Science Foundation under grant DMR-2143635. SS and LS acknowledge support from the U.S. Department of Energy, Nuclear Physics Quantum Horizons program through the Early Career Award DE-SC0021892.

[1] J. C. Y. Teo and C. L. Kane, Topological defects and gapless modes in insulators and superconductors, *Phys. Rev. B* **82**, 115120 (2010).

[2] R. Jackiw and C. Rebbi, Solitons with fermion number $\frac{1}{2}$, *Phys. Rev. D* **13**, 3398 (1976).

[3] R. Jackiw and P. Rossi, Zero modes of the vortex-fermion system, *Nuclear Physics B* **190**, 681 (1981).

[4] C.-Y. Hou, C. Chamon, and C. Mudry, Electron fractionalization in two-dimensional graphenelike structures, *Phys. Rev. Lett.* **98**, 186809 (2007).

[5] G. Moore and N. Read, Nonabelions in the fractional quantum hall effect, *Nuclear Physics B* **360**, 362 (1991).

[6] N. Read and D. Green, Paired states of fermions in two dimensions with breaking of parity and time-reversal symmetries and the fractional quantum hall effect, *Phys. Rev. B* **61**, 10267 (2000).

[7] D. A. Ivanov, Non-abelian statistics of half-quantum vortices in p -wave superconductors, *Phys. Rev. Lett.* **86**, 268 (2001).

[8] P. Fendley, Parafermionic edge zero modes in z_n -invariant spin chains, *Journal of Statistical Mechanics: Theory and Experiment* **2012**, P11020 (2012).

[9] P. Fendley, Strong zero modes and eigenstate phase transitions in the XYZ/interacting majorana chain, *Journal of Physics A: Mathematical and Theoretical* **49**, 30LT01 (2016).

[10] J. Cayssol, B. Dóra, F. Simon, and R. Moessner, Floquet topological insulators, *physica status solidi (RRL) - Rapid Research Letters* **7**, 101 (2013).

[11] M. S. Rudner and N. H. Lindner, Band structure engineering and non-equilibrium dynamics in floquet topological insulators, *Nature Reviews Physics* **2**, 229 (2020).

[12] K. Sacha and J. Zakrzewski, Time crystals: a review, *Reports on Progress in Physics* **81**, 016401 (2017).

[13] D. V. Else, C. Monroe, C. Nayak, and N. Y. Yao, Discrete time crystals, *Annual Review of Condensed Matter Physics* **11**, 467 (2020).

[14] V. Khemani, R. Moessner, and S. L. Sondhi, *A brief history of time crystals* (2019).

[15] J. Zhang, P. W. Hess, A. Kyprianidis, P. Becker, A. Lee, J. Smith, G. Pagano, I.-D. Potirniche, A. C. Potter, A. Vishwanath, N. Y. Yao, and C. Monroe, Observation of a discrete time crystal, *Nature* **543**, 217 (2017).

[16] S. Choi, J. Choi, R. Landig, G. Kucsko, H. Zhou, J. Isoya, F. Jelezko, S. Onoda, H. Sumiya, V. Khemani, C. von Keyserlingk, N. Y. Yao, E. Demler, and M. D. Lukin, Observation of discrete time-crystalline order in a disordered dipolar many-body system, *Nature* **543**, 221 (2017).

[17] A. Kyprianidis, F. Machado, W. Morong, P. Becker, K. S. Collins, D. V. Else, L. Feng, P. W. Hess, C. Nayak, G. Pagano, N. Y. Yao, and C. Monroe, Observation of a prethermal discrete time crystal, *Science* **372**, 1192 (2021).

[18] X. Mi, M. Ippoliti, C. Quintana, A. Greene, Z. Chen, J. Gross, F. Arute, K. Arya, J. Atalaya, R. Babbush, J. C. Bardin, J. Basso, A. Bengtsson, A. Bilmes, A. Bourassa, L. Brill, M. Broughton, B. B. Buckley, D. A. Buell, B. Burkett, N. Bushnell, B. Chiaro, R. Collins, W. Courtney, D. Debroy, S. Demura, A. R. Derk, A. Dunsworth, D. Eppens, C. Erickson, E. Farhi, A. G. Fowler, B. Foxen, C. Gidney, M. Giustina, M. P. Harrigan, S. D. Harrington, J. Hilton, A. Ho, S. Hong, T. Huang, A. Huff, W. J. Huggins, L. B. Ioffe, S. V. Isakov, J. Iveland, E. Jeffrey, Z. Jiang, C. Jones, D. Kafri, T. Khattar, S. Kim, A. Kitaev, P. V. Klimov, A. N. Korotkov, F. Kostritsa, D. Landhuis, P. Laptev, J. Lee, K. Lee, A. Locharla, E. Lucero, O. Martin, J. R. McClean, T. McCourt, M. McEwen, K. C. Miao, M. Mohseni, S. Montazeri, W. Mruczkiewicz, O. Naaman, M. Neeley, C. Neill, M. Newman, M. Y. Niu, T. E. O'Brien, A. Opremcak, E. Ostby, B. Pato, A. Petukhov, N. C. Rubin, D. Sank, K. J. Satzinger, V. Shvarts, Y. Su, D. Strain, M. Szalay, M. D. Trevithick, B. Villalonga, T. White, Z. J. Yao, P. Yeh, J. Yoo, A. Zalcman, H. Neven, S. Boixo, V. Smelyanskiy, A. Megrant, J. Kelly, Y. Chen, S. L. Sondhi, R. Moessner, K. Kechedzhi, V. Khemani, and P. Roushan, Time-crystalline eigenstate order on a quantum processor, *Nature* **601**, 531 (2021).

[19] P. T. Dumitrescu, J. G. Bohnet, J. P. Gaebler, A. Hankin, D. Hayes, A. Kumar, B. Neyenhuis, R. Vasseur, and

A. C. Potter, Dynamical topological phase realized in a trapped-ion quantum simulator, *Nature* **607**, 463 (2022).

[20] X. Zhang, W. Jiang, J. Deng, K. Wang, J. Chen, P. Zhang, W. Ren, H. Dong, S. Xu, Y. Gao, F. Jin, X. Zhu, Q. Guo, H. Li, C. Song, A. V. Gorshkov, T. Iadecola, F. Liu, Z.-X. Gong, Z. Wang, D.-L. Deng, and H. Wang, Digital quantum simulation of floquet symmetry-protected topological phases, *Nature* **607**, 468 (2022).

[21] J. W. McIver, B. Schulte, F.-U. Stein, T. Matsuyama, G. Jotzu, G. Meier, and A. Cavalleri, Light-induced anomalous hall effect in graphene, *Nature Physics* **16**, 38 (2019).

[22] M. Thakurathi, A. A. Patel, D. Sen, and A. Dutta, Floquet generation of majorana end modes and topological invariants, *Phys. Rev. B* **88**, 155133 (2013).

[23] M. S. Rudner, N. H. Lindner, E. Berg, and M. Levin, Anomalous edge states and the bulk-edge correspondence for periodically driven two-dimensional systems, *Phys. Rev. X* **3**, 031005 (2013).

[24] V. Khemani, A. Lazarides, R. Moessner, and S. L. Sondhi, Phase structure of driven quantum systems, *Phys. Rev. Lett.* **116**, 250401 (2016).

[25] D. V. Else, B. Bauer, and C. Nayak, Floquet time crystals, *Phys. Rev. Lett.* **117**, 090402 (2016).

[26] D. V. Else and C. Nayak, Classification of topological phases in periodically driven interacting systems, *Phys. Rev. B* **93**, 201103 (2016).

[27] C. W. von Keyserlingk and S. L. Sondhi, Phase structure of one-dimensional interacting floquet systems. i. abelian symmetry-protected topological phases, *Phys. Rev. B* **93**, 245145 (2016).

[28] H. B. Nielsen and M. Ninomiya, Absence of Neutrinos on a Lattice. 1. Proof by Homotopy Theory, *Nucl. Phys. B* **185**, 20 (1981), [Erratum: Nucl.Phys.B 195, 541 (1982)].

[29] H. B. Nielsen and M. Ninomiya, Absence of Neutrinos on a Lattice. 2. Intuitive Topological Proof, *Nucl. Phys. B* **193**, 173 (1981).

[30] D. B. Kaplan, A Method for simulating chiral fermions on the lattice, *Phys. Lett. B* **288**, 342 (1992), arXiv:hep-lat/9206013.

[31] Y. Shamir, Chiral fermions from lattice boundaries, *Nucl. Phys. B* **406**, 90 (1993), arXiv:hep-lat/9303005.

[32] P. H. Ginsparg and K. G. Wilson, A remnant of chiral symmetry on the lattice, *Phys. Rev. D* **25**, 2649 (1982).

[33] H. Neuberger, Exactly massless quarks on the lattice, *Phys. Lett. B* **417**, 141 (1998), arXiv:hep-lat/9707022.

[34] H. Neuberger, More about exactly massless quarks on the lattice, *Phys. Lett. B* **427**, 353 (1998), arXiv:hep-lat/9801031.

[35] J. Kogut and L. Susskind, Hamiltonian formulation of wilson's lattice gauge theories, *Phys. Rev. D* **11**, 395 (1975).

[36] X.-Q. Sun, M. Xiao, T. Bzdušek, S.-C. Zhang, and S. Fan, Three-dimensional chiral lattice fermion in floquet systems, *Phys. Rev. Lett.* **121**, 196401 (2018).

[37] M. DeMarco and X.-G. Wen, A single right-moving free fermion mode on an ultra-local 1 + 1d spacetime lattice (2018), arXiv:1805.03663 [hep-lat].

[38] Unless indicated otherwise, we restrict our focus in this work to single-particle spectral properties rather than many-body ones.

[39] D. Bödeker, G. D. Moore, and K. Rummukainen, Chern-simons number diffusion and hard thermal loops on the lattice, *Phys. Rev. D* **61**, 056003 (2000).

[40] J. Ambjorn, T. Askgaard, H. Porter, and M. E. Shaposhnikov, Sphaleron transitions and baryon asymmetry: A Numerical real time analysis, *Nucl. Phys. B* **353**, 346 (1991).

[41] G. Aarts and J. Smit, Real time dynamics with fermions on a lattice, *Nucl. Phys. B* **555**, 355 (1999), arXiv:hep-ph/9812413.

[42] Z.-G. Mou, P. M. Saffin, and A. Tranberg, Ensemble fermions for electroweak dynamics and the fermion pre-heating temperature, *JHEP* **11**, 097, arXiv:1307.7924 [hep-ph].

[43] L. H. Karsten, Lattice Fermions in Euclidean Space-time, *Phys. Lett. B* **104**, 315 (1981).

[44] Typical lattice Monte Carlo studies of quantum field theories are performed in Euclidean space-time. For real-time formulations path integrals for quantum field theories and quantum mechanical systems see [58–63].

[45] W. P. Su, J. R. Schrieffer, and A. J. Heeger, Solitons in polyacetylene, *Phys. Rev. Lett.* **42**, 1698 (1979).

[46] A. C. Potter, T. Morimoto, and A. Vishwanath, Classification of interacting topological floquet phases in one dimension, *Phys. Rev. X* **6**, 041001 (2016).

[47] See Supplemental Material.

[48] T. Iadecola, S. Sen, and L. Sivertsen, in preparation.

[49] H. C. Po, L. Fidkowski, A. Vishwanath, and A. C. Potter, Radical chiral floquet phases in a periodically driven kitaev model and beyond, *Phys. Rev. B* **96**, 245116 (2017).

[50] T. Kitagawa, E. Berg, M. Rudner, and E. Demler, Topological characterization of periodically driven quantum systems, *Phys. Rev. B* **82**, 235114 (2010).

[51] F. Nathan and M. S. Rudner, Topological singularities and the general classification of floquet–bloch systems, *New Journal of Physics* **17**, 125014 (2015).

[52] D. Carpentier, P. Delplace, M. Fruchart, and K. Gawędzki, Topological index for periodically driven time-reversal invariant 2d systems, *Phys. Rev. Lett.* **114**, 106806 (2015).

[53] M. Fruchart, Complex classes of periodically driven topological lattice systems, *Phys. Rev. B* **93**, 115429 (2016).

[54] M. F. L. Golterman, K. Jansen, and D. B. Kaplan, Chern-Simons currents and chiral fermions on the lattice, *Phys. Lett. B* **301**, 219 (1993), arXiv:hep-lat/9209003.

[55] P. Ponte, A. Chandran, Z. Papić, and D. A. Abanin, Periodically driven ergodic and many-body localized quantum systems, *Annals of Physics* **353**, 196 (2015).

[56] L. D'Alessio and M. Rigol, Long-time behavior of isolated periodically driven interacting lattice systems, *Phys. Rev. X* **4**, 041048 (2014).

[57] D. V. Else, B. Bauer, and C. Nayak, Prethermal phases of matter protected by time-translation symmetry, *Phys. Rev. X* **7**, 011026 (2017).

[58] G. Kanwar and M. L. Wagman, Real-time lattice gauge theory actions: Unitarity, convergence, and path integral contour deformations, *Phys. Rev. D* **104**, 014513 (2021), arXiv:2103.02602 [hep-lat].

[59] A. Alexandru, G. Basar, P. F. Bedaque, S. Vartak, and N. C. Warrington, Monte Carlo Study of Real Time Dynamics on the Lattice, *Phys. Rev. Lett.* **117**, 081602 (2016), arXiv:1605.08040 [hep-lat].

[60] S. Lawrence and Y. Yamauchi, Normalizing Flows and the Real-Time Sign Problem, *Phys. Rev. D* **103**, 114509 (2021), arXiv:2101.05755 [hep-lat].

[61] Y. Tanizaki and T. Koike, Real-time Feynman path in-

tegral with Picard–Lefschetz theory and its applications to quantum tunneling, *Annals Phys.* **351**, 250 (2014), arXiv:1406.2386 [math-ph].

[62] A. Alexandru, G. Basar, P. F. Bedaque, and G. W. Ridgway, Schwinger-Keldysh formalism on the lattice: A faster algorithm and its application to field theory, *Phys. Rev. D* **95**, 114501 (2017), arXiv:1704.06404 [hep-lat].

[63] Z.-G. Mou, P. M. Saffin, A. Tranberg, and S. Woodward, Real-time quantum dynamics, path integrals and the method of thimbles, *JHEP* **06**, 094, arXiv:1902.09147 [hep-lat].

Supplemental materials for “Floquet insulators and lattice fermions”

Thomas Iadecola,^{1,2,*} Srimoyee Sen,^{1,†} and Lars Sivertsen^{1,‡}

¹*Department of Physics and Astronomy, Iowa State University, Ames, Iowa 50011, USA*

²*Ames National Laboratory, Ames, Iowa 50011, USA*

(Dated: June 30, 2023)

QUASIENERGY SPECTRUM OF U_F

In this section we will derive the quasienergy spectrum of the bulk Floquet Hamiltonian defined as

$$H_F = -\text{Im}[\log U_F] = -\text{Im}[\log(\exp(-iH_1 t_1) \exp(-iH_0 t_0))], \quad (\text{S1})$$

where the SSH-Hamiltonians H_i are defined as

$$\begin{aligned} H_0 &= 2 \sum_{j=0}^{N-1} (a_{2j}^\dagger a_{2j+1} + \text{H.c.}) \\ H_1 &= 2 \sum_{j=0}^{N-1} (a_{2j+1}^\dagger a_{2j+2} + \text{H.c.}). \end{aligned} \quad (\text{S2})$$

Since we are considering the bulk spectrum, we have in the above and will in what follows assume periodic boundary conditions, $a_{2N} = a_0$. We define

$$a_{2j} = c_{2j}, \quad a_{2j+1} = d_{2j+1}. \quad (\text{S3})$$

We proceed by performing a Fourier transform

$$\begin{aligned} c_{2j} &= \frac{1}{\sqrt{N}} \sum_k e^{2ikj} c_k, \\ d_{2j+1} &= \frac{1}{\sqrt{N}} \sum_k e^{+ik(2j+1)} d_k, \end{aligned} \quad (\text{S4})$$

where $0 \leq k < \pi$. The Hamiltonian written in momentum space are of the form

$$\begin{aligned} H_0 &= 2 \sum_k (c_k^\dagger d_k e^{ik} + \text{H.c.}), \\ H_1 &= 2 \sum_k (c_k^\dagger d_k e^{-ik} + \text{H.c.}) \end{aligned} \quad (\text{S5})$$

which can be rewritten in matrix form as

$$\begin{aligned} H_0 &= 2 \begin{pmatrix} 0 & e^{ik} \\ e^{-ik} & 0 \end{pmatrix} = 2\sigma_x \cos k - 2\sigma_y \sin k \equiv 2\boldsymbol{\sigma} \cdot \mathbf{n}_0, \\ H_1 &= 2 \begin{pmatrix} 0 & e^{-ik} \\ e^{ik} & 0 \end{pmatrix} = 2\sigma_x \cos k + 2\sigma_y \sin k \equiv 2\boldsymbol{\sigma} \cdot \mathbf{n}_1. \end{aligned} \quad (\text{S6})$$

Here σ_i are the Pauli spin matrices, and

$$\mathbf{n}_0 = \begin{pmatrix} \cos k \\ -\sin k \end{pmatrix}, \quad \mathbf{n}_1 = \begin{pmatrix} \cos k \\ \sin k \end{pmatrix}, \quad \boldsymbol{\sigma} = \begin{pmatrix} \sigma_x \\ \sigma_y \end{pmatrix}. \quad (\text{S7})$$

Using the relation

$$\exp(-i\theta(\boldsymbol{\sigma} \cdot \mathbf{n})) = \cos(\theta) - i(\boldsymbol{\sigma} \cdot \mathbf{n}) \sin(\theta), \quad (\text{S8})$$

we advance towards finding the eigenvalues of the Floquet operator by inserting the expressions for H_0 and H_1 into (S1):

$$\begin{aligned} U_F &= \exp(-iH_1 t_1) \exp(-iH_0 t_0) \\ &= \exp(-2it_1(\boldsymbol{\sigma} \cdot \mathbf{n}_1)) \exp(-2it_0(\boldsymbol{\sigma} \cdot \mathbf{n}_0)) \end{aligned} \quad (S9)$$

From here one can find the eigenvalues of U_F

$$\begin{aligned} \lambda &= \frac{1}{4} \left[\cos(2k - 2t_0 - 2t_1) + 2 \cos(2t_0 - 2t_1) - \cos(2k + 2t_0 - 2t_1) \right. \\ &\quad \left. - \cos(2k - 2t_0 + 2t_1) + 2 \cos(2t_0 + 2t_1) + \cos(2k + 2t_0 + 2t_1) \right] \\ &\pm i \left\{ 1 - \frac{1}{16} [\cos(2k - 2t_0 - 2t_1) + 2 \cos(2t_0 - t_1) - \cos(2k + 2t_0 - 2t_1) \right. \\ &\quad \left. - \cos(2k - 2t_0 + 2t_1) + 2 \cos(2t_0 + 2t_1) + \cos(2k + 2t_0 + 2t_1)]^2 \right\}^{1/2} \\ &\equiv e^{\pm i\theta}. \end{aligned} \quad (S10)$$

We can now obtain the eigenvalues of the Floquet Hamiltonian H_F given by

$$\begin{aligned} \lambda_{H_F} &= \pm \theta \\ &= \pm \arccos \left\{ \frac{1}{4} [\cos(2k - 2t_0 - 2t_1) + 2 \cos(2t_0 - 2t_1) - \cos(2k + 2t_0 - 2t_1) \right. \\ &\quad \left. - \cos(2k - 2t_0 + 2t_1) + 2 \cos(2t_0 + 2t_1) + \cos(2k + 2t_0 + 2t_1)] \right\}. \end{aligned} \quad (S11)$$

In particular, note that for $t_0 = \frac{\pi}{4}$ we have

$$\lambda_{H_F} = \pm \arccos \left[-\sin(2t_1) \cos(2k) \right]. \quad (S12)$$

The \arccos function has the feature

$$\arccos(-x) = \pi - \arccos(x), \quad (S13)$$

and therefore, for a fixed value of t_1 , there is a π pairing in the eigenvalues of H_F , i.e. if there is an eigenvalue $\lambda_{H_F} = \kappa$, there is another one at $\pi/T - \kappa$. This follows as k takes values from 0 to π . Furthermore, note that if we instead let $t_1 = \pi/4$, we get the exact same result, except $t_0 \rightarrow t_1$. Hence there is also π pairing along the $t_1 = \pi/4$ line. However, this pairing disappears with OBC, as the phases along this line have either zero or π modes on the boundary, not both—the line $\frac{t_0}{T} = \frac{\pi}{4}$ is therefore the only region of the phase diagram with π -pairing independent of boundary conditions, so it is there that we expect the cleanest relationship between the Floquet and lattice-fermion models.

PHASES OF U_F

In this section we discuss the phase diagram of the Floquet operator

$$U_F = e^{-iH_1 t_1} e^{-iH_0 t_0}, \quad (S14)$$

where

$$\begin{aligned} H_0 &= 2 \sum_{j=0}^{N-1} (a_{2j}^\dagger a_{2j+1} + \text{H.c.}) \\ H_1 &= 2 \sum_{j=0}^{N-2} (a_{2j+1}^\dagger a_{2j+2} + \text{H.c.}) \end{aligned} \quad (S15)$$

Note that we have written the model with open boundary conditions to facilitate distinguishing the four phases by their edge modes. In this section we will work in units such that $T = 1$. This model is directly analogous to the ‘‘Class D’’ toy model of Ref. [?], with the exception that the latter is composed of Majorana fermions instead of complex fermions. We follow closely the analysis of Ref. [?]. The strategy is to characterize U_F along the representative lines $t_0 = 0$, $t_1 = 0$, $t_0 = \pi/2$, and $t_1 = \pi/2$. Standard continuity arguments then imply that any point in parameter space that can be reached from these lines without closing the quasienergy gap must be in the same phase.

Trivial and 0 phases

The trivial and 0 phases are closely related to their undriven counterparts. The trivial phase is smoothly connected to the line $t_1 = 0$, where U_F reduces to evolution under the trivial Hamiltonian H_0 , which hybridizes all lattice sites in pairs. The 0 phase is smoothly connected to the line $t_0 = 0$, where U_F reduces to evolution under the topological Hamiltonian H_1 , which hybridizes bulk sites while leaving the edge sites 0 and $2N - 1$ decoupled.

0 π phase

To understand the 0π phase, it is useful to rewrite H_0 and H_1 via a Jordan-Wigner transformation as

$$H_0 = \sum_{j=0}^{N-1} (X_{2j}X_{2j+1} + Y_{2j}Y_{2j+1}) \quad (\text{S16})$$

$$H_1 = \sum_{j=0}^{N-2} (X_{2j+1}X_{2j+2} + Y_{2j+1}Y_{2j+2}). \quad (\text{S17})$$

We then consider U_F along the line $t_1 = \pi/2$:

$$U_F = e^{-i\frac{\pi}{2}H_1} e^{-iH_0 t_0} \quad (\text{S18})$$

$$= \prod_{j=0}^{N-2} Z_{2j+1}Z_{2j+2} e^{-iH_0 t_0} \quad (\text{S19})$$

$$= U_{\text{edge}} e^{-it_0(X_0X_1+Y_0Y_1+X_{2N-2}X_{2N-1}+Y_{2N-2}Y_{2N-1})} Q U_{\text{bulk}} \quad (\text{S20})$$

where $U_{\text{edge}} = Z_0Z_{2N-1}$, $Q = \prod_{j=0}^{N-1} Z_{2j}Z_{2j+1}$, $U_{\text{bulk}} = \prod_{j=1}^{N-2} e^{-it_0(X_{2j}X_{2j+1}+Y_{2j}Y_{2j+1})}$, and where we have used the identity

$$e^{-i\frac{\pi}{2}H_1} = \prod_{j=0}^{N-2} e^{-i\frac{\pi}{2}(X_{2j+1}X_{2j+2}+Y_{2j+1}Y_{2j+2})} \quad (\text{S21})$$

$$= \prod_{j=0}^{N-2} e^{-i\frac{\pi}{2}X_{2j+1}X_{2j+2}} e^{-i\frac{\pi}{2}Y_{2j+1}Y_{2j+2}} \quad (\text{S22})$$

$$= - \prod_{j=0}^{N-2} X_{2j+1}X_{2j+2}Y_{2j+1}Y_{2j+2} \quad (\text{S23})$$

$$= \prod_{j=0}^{N-2} Z_{2j+1}Z_{2j+2}. \quad (\text{S24})$$

Note that Q constitutes a global symmetry as it commutes with H_0 and H_1 . Next, we transform Eq. (S20) by the unitary operator

$$W = e^{i\frac{t_0}{2}(X_0X_1+Y_0Y_1+X_{2N-2}X_{2N-1}+Y_{2N-2}Y_{2N-1})}, \quad (\text{S25})$$

which commutes with Q , U_{edge} , and U_{bulk} , to obtain

$$\tilde{U}_{\text{F}} = W^{\dagger} U_{\text{F}} W = W^{\dagger} U_{\text{edge}} e^{-it_0(X_0 X_1 + Y_0 Y_1 + X_{2N-2} X_{2N-1} + Y_{2N-2} Y_{2N-1})} W Q U_{\text{bulk}} \quad (\text{S26})$$

$$= U_{\text{edge}} W e^{-it_0(X_0 X_1 + Y_0 Y_1 + X_{2N-2} X_{2N-1} + Y_{2N-2} Y_{2N-1})} W U_{\text{bulk}} \quad (\text{S27})$$

$$= U_{\text{edge}} Q U_{\text{bulk}}, \quad (\text{S28})$$

where we used that U_{edge} anticommutes with the generator of W . This demonstrates that the quasienergy spectrum of U_{F} factors into the product of the spectra of the commuting unitaries U_{edge} , Q , and U_{bulk} . Eigenstates can be labeled uniquely by their eigenvalues under the commuting quantities U_{edge} , Q , U_{bulk} , and under the additional bulk symmetry operator $P_{\text{bulk}} = \prod_{j=1}^{N-2} X_{2j} X_{2j+1}$ and edge symmetry operator $P_{\text{edge}} = X_0 X_1 X_{2N-2} X_{2N-1}$.

To see how 0 and π modes emerge, let us denote a reference eigenstate of \tilde{U}_{F} by $|u_{\text{edge}}, p_{\text{edge}}, p_{\text{bulk}}, q, E\rangle$, where E is an energy eigenvalue of $H_{\text{bulk}} = \sum_{j=1}^{N-2} (X_{2j} X_{2j+1} + Y_{2j} Y_{2j+1})$ and where $u_{\text{edge}}, p_{\text{edge}}, p_{\text{bulk}}, q = \pm 1$ are eigenvalues of U_{edge} , P_{edge} , P_{bulk} , and Q , respectively. (Note that all of these operators mutually commute with one another; we will therefore call them symmetries of U_{F} .) Denote the quasienergy of this reference state by $\epsilon = i \ln(u_{\text{edge}} q e^{-iE t_0})$. We can toggle between the four joint eigenstates of the edge operators U_{edge} and P_{edge} by acting with the operators Z_0 , which anticommutes with P_{edge} and commutes with all other symmetries, and $X_0 X_1$, which anticommutes with U_{edge} and commutes with all other symmetries. This generates the following “ 0π -multiplet” of states:

State	Quasienergy
$ u_{\text{edge}}, p_{\text{edge}}, p_{\text{bulk}}, q, E\rangle$	ϵ
$Z_0 u_{\text{edge}}, p_{\text{edge}}, p_{\text{bulk}}, q, E\rangle = u_{\text{edge}}, -p_{\text{edge}}, p_{\text{bulk}}, q, E\rangle$	ϵ
$X_0 X_1 u_{\text{edge}}, p_{\text{edge}}, p_{\text{bulk}}, q, E\rangle = -u_{\text{edge}}, p_{\text{edge}}, p_{\text{bulk}}, q, E\rangle$	$\epsilon + \pi$
$Y_0 X_1 u_{\text{edge}}, p_{\text{edge}}, p_{\text{bulk}}, q, E\rangle = -u_{\text{edge}}, -p_{\text{edge}}, p_{\text{bulk}}, q, E\rangle$	$\epsilon + \pi$

We refer to Z_0 as a zero-mode operator since it commutes with U_{F} , and $X_0 X_1$ as a π -mode operator because it anticommutes with U_{F} . Note that there is another zero- and π -mode operator at the other end of the chain: $Z_{2N-1} = U_{\text{edge}} Z_0$ and $X_{2N-2} X_{2N-1} = P_{\text{edge}} X_0 X_1$. Thus we could have alternatively chosen to label states in this multiplet by, say, eigenvalues of Z_0 and Z_{2N-1} instead of U_{edge} and P_{edge} , and to toggle between these eigenvalues with $X_0 X_1$ and $X_{2N-2} X_{2N-1}$.

π phase

The π phase can be treated similarly to the 0π phase. Here we consider the representative point $t_0 = \pi/2$, where

$$U_{\text{F}} = e^{-iH_1 t_1} e^{-i\frac{\pi}{2} H_0} \quad (\text{S29})$$

$$= e^{-iH_1 t_1} Q \quad (\text{S30})$$

$$= e^{-iH_1 t_1} \left(\prod_{j=0}^{N-2} Z_{2j+1} Z_{2j+2} \right) Z_0 Z_{2N-1} \quad (\text{S31})$$

$$= e^{-iH_1(t_1 + \frac{\pi}{2})} Z_0 Z_{2N-1} \quad (\text{S32})$$

$$= U_{\text{bulk}} U_{\text{edge}}, \quad (\text{S33})$$

where we have used Eq. (S21). Note that the resulting model also has the global symmetry $P = \prod_{j=0}^{2N-1} X_{2j} X_{2j+1}$ with eigenvalues $p = \pm 1$. We can repeat the analysis of the 0π phase to demonstrate the existence of π modes. To do this, let $|u_{\text{edge}}, p, E\rangle$ be a reference eigenstate labeled by the symmetry eigenvalues $u_{\text{edge}}, p = \pm 1$ and an energy eigenvalue E of H_1 . The associated quasienergy is $\epsilon = i \ln(u_{\text{edge}} e^{-iE t_1})$. The eigenvalues of U_{edge} can be toggled by the π -mode operator X_0 , leading to the following “ π -doublet”:

State	Quasienergy
$ u_{\text{edge}}, p, E\rangle$	ϵ
$X_0 u_{\text{edge}}, p, E\rangle = -u_{\text{edge}}, p, E\rangle$	$\epsilon + \pi$

Mapping to two copies of the Majorana model

A simpler way to verify that the phase diagram of U_F matches that of the Majorana model of Ref. [?] is to observe that the former amounts to two copies of the latter. To see this we write the complex fermions a_j in terms of Majorana fermions α_j, β_j in the standard way:

$$a_j = \frac{1}{2}(\alpha_j + i\beta_j). \quad (\text{S34})$$

Substituting this into Eq. (S15) gives

$$\begin{aligned} H_0 &= \sum_{j=0}^{N-1} (i\alpha_{2j}\beta_{2j+1} - i\beta_{2j}\alpha_{2j+1}) \\ H_1 &= \sum_{j=0}^{N-2} (i\alpha_{2j+1}\beta_{2j+2} - i\beta_{2j+1}\alpha_{2j+2}). \end{aligned} \quad (\text{S35})$$

This is precisely two copies of the aforementioned Majorana model, with one of the copies time-reversed with respect to the other. We note that the two copies are not strictly independent, since performing a $U(1)$ transformation on the complex fermions leads to a nontrivial mixing of the Majorana operators:

$$a_j \rightarrow e^{i\theta} a_j = (\cos \theta \alpha_j + \sin \theta \beta_j) + i(\sin \theta \alpha_j - \cos \theta \beta_j). \quad (\text{S36})$$

This mixing is necessary in order for the two copies of the Majorana model to manifest the $U(1)$ symmetry of the complex-fermion model.

DOMAIN WALL IN η IN THE WILSON-DIRAC MODEL

Here we consider a spatially dependent Wilson-Dirac Hamiltonian with a domain wall in the parameter $\eta = \frac{t_1}{T} - \frac{\pi}{4}$ that tunes between the trivial and 0π phases. To implement this we pick the following domain wall configuration with + and - subscripts denoting the regions $x_1 > 0$ and < 0

$$\begin{aligned} m_{\pm} &= -\sin(2\eta_{\pm}) \\ R_{\pm} &= \frac{1 + \sin(2\eta_{\pm})}{2} \\ \eta_+ &= -\eta_- > 0. \end{aligned} \quad (\text{S37})$$

We can now look for edge modes on the domain wall by solving the equation of motion

$$(-iR\gamma_1\nabla_1 + m - \frac{R}{2}\nabla_1^2)\psi = 0 \quad (\text{S38})$$

with $\gamma_0 = \sigma_2$ and $\gamma_1 = -i\sigma_1$ and m and R are spatially dependent, i.e. taking the above specified values for $x_1 > 0$ and < 0 . We can solve this EOM with an ansatz of

$$\psi = \begin{pmatrix} 1 \\ 1 \end{pmatrix} \varphi \quad (\text{S39})$$

which reduces the EOM to

$$\begin{aligned} -\frac{\varphi(x_1 + 1) - \varphi(x_1 - 1)}{2} + \frac{m}{R}\varphi - \frac{\varphi(x_1 + 1) + \varphi(x_1 - 1) - 2\varphi(x_1)}{2} &= 0 \\ \implies \varphi(x_1 + 1) &= \left(1 + \frac{m}{R}\right)\varphi. \end{aligned} \quad (\text{S40})$$

So, we find normalizable solutions for all of the parameter space of interest, i.e. $\frac{\pi}{4} > \eta > 0$ given by

$$\begin{aligned} \varphi(x_1) &= \left(1 + \frac{m}{R}\right)^{x_1} \\ &= \begin{cases} \left(1 + \frac{m_+}{R_+}\right)^{x_1} & \text{for } x_1 > 0 \\ \left(1 + \frac{m_-}{R_-}\right)^{x_1} & \text{for } x_1 < 0. \end{cases} \end{aligned}$$

This corresponds to a localized mode with localization length

$$\xi_{\pm} = \frac{-1}{\ln \left(1 - \frac{|m_{\pm}|}{R_{\pm}} \right)} \quad (\text{S41})$$

to either side of the domain wall.